Digest Journal of Nanomaterials and Biostructures Vol. 19, No. 3, July -September 2024, p. 1159 - 1171

CoFe bimetallic phosphide fabricated by topological transformation strategy for efficient electrooxidation of benzyl alcohol

J. Y. Liu[a,#] H. J. Liu[a,#], Y. Q. Xu[a,b,c,*], H. Wang[d], L. J. Wang[a,b]
[a]*College of Materials Science and Engineering, Key Laboratory of New Processing Technology for Nonferrous Metals and Materials, Ministry of Education, Guilin University of Technology, Guilin 541004, China*
[b]*Collaborative Innovation Center for Exploration of Nonferrous Metal Deposits and Efficient Utilization of Resources, Guilin University of Technology, Guilin 541004, China*
[c]*Guangxi Key Laboratory of Nuclear Physics and Nuclear Technology, Guangxi Normal University, Guilin 541004, China*
[d]*College of Physics and Technology, Guangxi Normal University, Guilin 541004, China*

Rational design of effective non-precious metallic electrocatalysts is crucial for electrooxidation of benzyl alcohol (BA) producing benzoic acid (BAC). Herein, CoFe bimetallic phosphide (CoFeP-m) with bimetallic synergy, fully exposed active sites, and fast charge transfer was fabricated by topological transformation of CoFe-LDH for the efficient electrooxidation of BA to BAC under mild condition. Under the optimal conditions of starting voltage of 0.7 V *vs*. Ag/AgCl at 25ºC, CoFeP-300 achieved 97.71% transformation of BA and 97.84% BAC's selectivity for 8 h. In addition, CoFeP-300 showed excellent stability which maintained 95.89% transform into BA and 95.37% BAC's selectivity at the sixth cycle.

(Received March 6, 2024; Accepted August 1, 2024)

Keywords: Electrooxidation of benzyl alcohol, Transition metal phosphide, Topological transformation, Layered double hydroxide

1. Introduction

Benzaldehyde and benzoic acid (BAC) prepared by electrooxidation of benzyl alcohol (BA) is broadly used in fine chemical industry, medicinal chemistry and functional polymers [1]. At present, the high yield of BAC mainly depends on the oxidation process under high working potential, resulting in high electricity consumption that is not conducive to environmental protection requirements [2]. Electrooxidation of BA driven by low working potential is recognized as development trend. Therefore, the development of broad, selective, low-cost, and effective electrocatalysts at low working potential is desirable for the electrooxidation of BA.

Transition metal phosphides (TMPs) exhibit good stability and durability in acidic and alkaline media due to their metal-like properties and good electrical conductivity [3]. As such, TMPs possess excellent performance and potential in the field of electrochemistry. Phosphorus increases the distance between metal atoms, this results in the *d* band contracting and lessens the metal-atom interaction, narrowing the *d* band and bolstering the Fermi level state density [4]. Meanwhile, the *d* band center can be modulated to reduce the adsorption energy, thus promoting desorption and increasing the corresponding catalytic activity. For example, NiP [5], CoP [6], and Fe_2P [7] have shown excellent performance and potential in the field of electrocatalysis in acidic and alkaline media due to their unique structure [8]. However, the above TMPs are composed of single metal, which restrict the exposure of active websites and reduces the electrocatalytic reaction kinetics. Studies have shown that bimetallic and/or polymetallic TMPs can adsorb

# These authors contributed equally to this work.
* Corresponding author: xuyanqi@glut.edu.cn
https://doi.org/10.15251/DJNB.2024.193.1159

reaction intermediates better than mono-metallic TMPs due to the synergistic effect of metal ions [9-11]. Furthermore, polymetallic TMPs possess abundant metal-metal bonds and metal-phosphorus bonds, which make them showing better chemical stability and faster charge transfer rate than mono-metallic TMPs, resulting improved catalytic performance [12]. Although polymetallic TMPs have achieved good catalytic performance for the electrooxidation of BA, it is still difficult to preserve the catalytic activity for a long time, especially in alkaline solution, which seriously affects the catalytic activity of these polymetallic TMPs. Consequently, the development of TMPs catalysts for electrocatalysts with expense performance, outstanding performance, and superior stability is required [13].

In this context, layered double hydroxide (LDHs) [14], an example 2D framework that is two dimensions and has the overall concept $[M^{2+}_{1-x}M^{3+}_{x}(OH)_2](A^{n-})_{x/n}\cdot mH_2O$ [15], exhibiting unique ingredient and highly adjustable chemical composition, offer a versatile platform to produce polymetallic TMPs through topological transformation in reducing atmosphere. Polymetallic TMPs derived from LDHs show highly exposed active sites, optimal adsorption energy, and satisfactory stability for electrocatalysis [16, 17]. Furthermore, benefiting from the strong electrostatic interactions and compositional diversity of LDHs, functional complementarity and synergism between the active site and the co-metal in polymetallic TMPs can be realized, thus further regulating the redistribution of electrons, thereby improving the electron mobility [18, 19].

Herein, CoFe bimetallic phosphide (CoFeP-m) with bimetallic synergy, fully exposed active sites and fast charge transfer was synthetized by topological transformation of CoFe-LDH using NaH_2PO_2 as phosphating agents. The CoFeP-m showed excellent electrocatalytic performance of BA oxidation, where the 97.71% transform into BA and 97.84% BAC's selectivity over CoFeP-300 could be achieved at the operating voltage of 0.7 V *vs.* Ag/AgCl under the normal atmospheric temperature for 8 h. Following six cycles, the transform into BA and the BAC's selectivity maintained 95.89% and 95.37%, suggesting the excellent durability of the electrocatalyst. The study provides a new idea for electrooxidation of BA with TMPs materials.

2. Experimental

2.1. Materials

Formamide and $Fe(NO_3)_3\cdot 9H_2O$ were obtained from Aladdin Biochemistry Technology Co., Ltd.. $Co(NO_3)_2\cdot 6H_2O$, NaH_2PO_2, and benzyl alcohol (BA,99%), KOH, NaOH and $NaNO_3$ were purchased from Rhawn Chemical Reagent Co., Ltd. and Xilong Chemical Reagent Co., Ltd. respectively. All the above aforementioned substances were not pretreated.

2.2. Characterizations

Comprehensive analyses of the individual characteristics of the sample were carried out through X- ray powder diffraction (XRD) (scanning speed was 5°/min, scanning range 2θ was 5-70°). Scanning electron microscope (SEM, Hitachi S-4800) and transmission electron microscope (TEM, JEM-2010F) were used to observe the morphology and structure of the samples. The surface area of (BET) was measured on TriStarll3200. It was characterized by Thermo Scientific Ka (XPS). Using a Thermo Nicolet NEXUS 670, (FT-IR) spectra were captured in the 4000-400 cm^{-1} region.

2.3. Preparation of CoFe-LDH and CoFeP-m (m = 250, 300, and 350)

CoFe-LDH was prepared by simple and rapid hydrothermal synthesis [20]. Add 0.2 mmol $Fe(NO_3)_3\cdot 9H_2O$ and 0.6 mmol $Co(NO_3)_2\cdot 6H_2O$ into 10ml deionized water to obtain solution A. Under the condition of constant temperature of 80℃ and stirring, the A solution and 0.02 M NaOH solution were added concurrently to a 10 mL $NaNO_3$ (0.2 mmol) mixture comprising 23 volume% formamide. After titration, the obtained precipitate, e.g. CoFe-LDH, was washed by centrifugation and dried at 60 °C.

The CoFeP-m (m = 250, 300, and 350) were prepared by topological transformation of CoFe-LDH. In a typical procedure 20 mg CoFe-LDH and 1.0 g NaH_2PO_2 were respectively spread flat on the bottom of two quartz porcelain boats which were placed in a tube furnace at a distance

of 2 cm. Specially, NaH_2PO_2 and CoFe-LDH were placed in the upper and decrease tuyeres of the tubular furnace respectively. The CoFe-LDH had been warmed in an Ar environment for three hours at 250°C, 300°C, and 350°C at a rate of 5°C per minute. The samples were expressed as CoFeP-m (m = 250, 300, and 350).

2.4. Electrochemical measurements

The electrochemical work measurement adopts the electrochemical workstation (CHI660e) of the standard three-electrode system. Among the three electrodes, the working electrode, the reference electrode and the counter electrode are: CoFeP-m (m = 250, 300, and 350), Ag/AgCl and platinum net respectively. The electrode for convert that measured potential into reversible hydrogen can be calculate by the formula $E_{RHE} = E_{Ag/AgCl}+0.059pH+0.197$. Cyclic voltammogram (CV) measurements were obtained in 1.0 M KOH with 1.0 M BA, within the voltage range of 0.4 V to 0.9 V at a scan rate of 50 mV/s. Linear sweep voltammetry (LSV) curves were measured in the voltage range 0-0.6V at the scanning rate is 5 mV/s. The frequency range for the electrochemical impedance spectroscopy (EIS) curves was 100 kHz to 0.01 Hz, and the voltage was set to 0.5 V. The catalysts' electrochemical active surface area (ECSA) was determined by measuring the CV at potentials between 0.25 and 0.35 V and speed of scanning between 2, 4, 6, 8, and 10 mV/s, and the computational formula can be expressed as $ECSA = C_{dl}/C_s$ (where C_s is the sample's specific capacitance and C_{dl} (double double-layer capacitance) is the CV curve's slope).

2.5. Electrooxidation of benzyl alcohol

BA was selectively removed by using H-type electrochemical cells split by a Nafion-117 membrane, with Pt mesh and CoFeP-LDH as electrodes. The anode cell utilized 35 mL of 1.0 M KOH and 10 mM BA solution, and the cathode cell used 35 mL of 1.0 M KOH solution. The electrochemical reduction of BA was done under the aforementioned circumstances for eight hours at ambient temperature. The liquid product was subjected to HPLC analysis using a Thermo Fisher U3000 equipped with an ultraviolet detector and C18(2) column. The mobile phase consisted of acetonitrile (volume ratio of $HCOOH/CH_3CN = 70 : 30$) and 0.02M formic acid aqueous solution, with a flow rate of 1 mL/min. The following definitions apply to the percent conversion of BA (C_{BA}) and the selectivity of its oxidative outcome:

$$C_{AB}(\%) = \frac{C_{BA}^0 - C_{BA}^t}{C_{BA}^0} \times 100\% \quad (1)$$

$$S_{BAC}(\%) = \frac{C_{BAC}}{C_{BAC}+C_{BAD}} \times 100\% \quad (2)$$

$$S_{BAD}(\%) = \frac{C_{BAD}}{C_{BAC}+C_{BAD}} \times 100\% \quad (3)$$

where C_{BA}^0 and are C_{BA}^t respectively represent the concentration of BA at the initial stage and at a certain reaction time, C_N (N = benzoic acid (BAC), benzaldehyde (BAD)) is the concentration of reaction products at a certain moment.

3. Results and discussion

The crystal framework of CoFe-LDH and CoFeP-m (m = 250, 300, and 350) were determined by XRD. According to Fig. 1a, the Bragg diffraction peaks were seen in the CoFe-LDH XRD spectrum at 11.64°, 23.42°, 34.07°, 35.11°, 46.23°, and 59.09°, respectively, which can be ascribed to the (003), (006), (012), (009), (018), and (110) typical LDHs' crystal framework, indicating that CoFe-LDH was successfully synthesized. The XRD patterns of the phosphatized samples (CoFeP-m (m = 250, 300, and 350)) exhibited diffraction peaks assigned to the (011), (201), (112), (202), (103), and (212) characteristic diffraction peaks of the orthorhombic CoP, which were much different from that of CoFe-LDH (Fig. 1b). When the phosphating temperature

is 250℃, the obtained CoFeP-250 exhibits an additional diffraction peak at ~ 45° in comparison with CoFeP-300 and CoFeP-350, which may be related to the reason that the CoFe-LDH precursor is not completely phosphatized. However, CoFeP-300 and CoFeP-350 have almost the same diffraction peaks, and both show the (011), (201), (112), (202), (103) and (212) characteristic diffraction peaks of the orthorhombic system CoP. It's worth noting that the in intensity of diffraction peaks of CoFeP-300 were weaken than those of CoFeP-250 and CoFeP-350, indicating CoFeP-300 has low crystallinity that possess large surface areas and more randomly oriented bonds, thus producing more surface-exposed defects as catalytic active sites. The nitrogen isothermal adsorption-desorption curve of CoFeP-300 showed obvious hysteresis loop (Fig. 1c-d), indicating that it has mesoporous characteristics. Furthermore, the specific surface area of CoFeP-300 was 11.32 $m^2 g^{-1}$, while the pore size distribution was 3.0-15.0 nm and the pore size was about 3.4 nm. Therefore, the pore structure promoted the dispersion of reacting substances and the transfer of charge in the electrochemical process, speeding up the kinetics of the electrooxidation of BA [21].

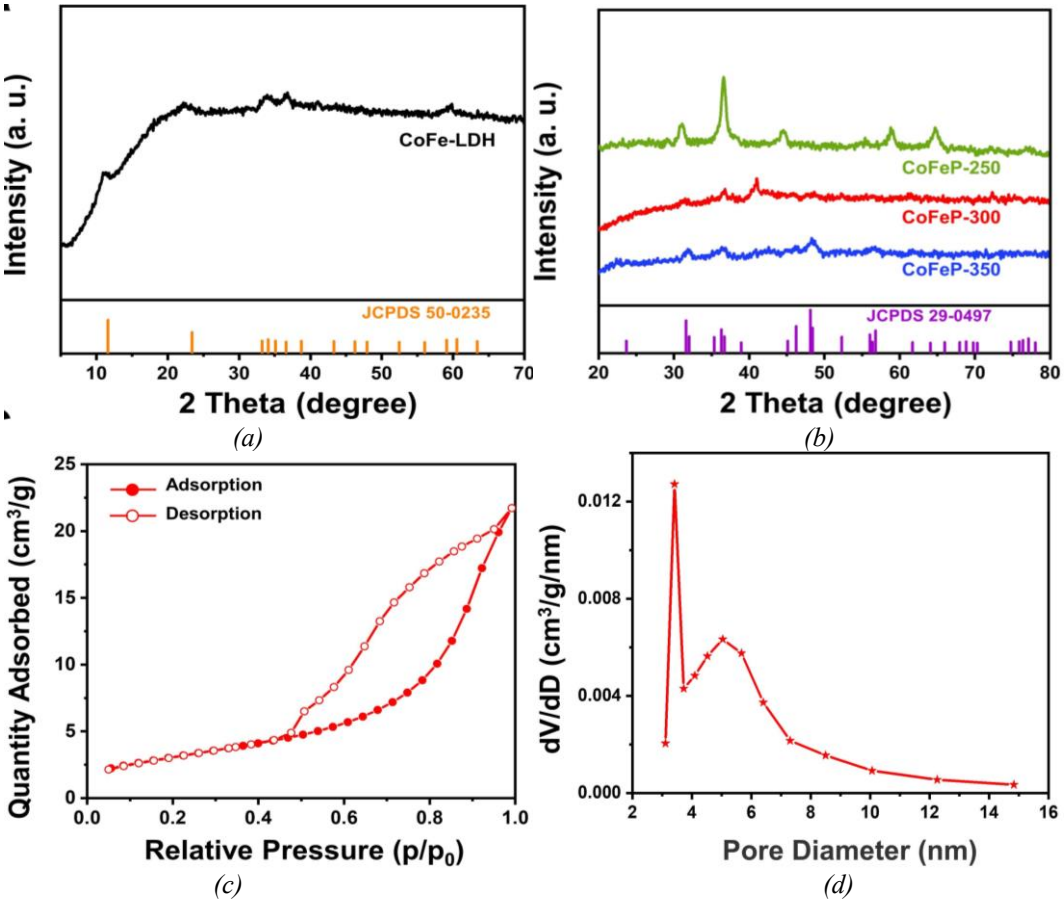

Fig. 1. XRD spectrum of CoFe-LDH(a). (b) XRD spectrum of CoFeP-m (m = 250, 300, and 350). (c) Adsorption-desorption isotherms for N2 and (d) the corresponding pore dimension distributions for CoFeP-300.

The surface morphology, element distribution, internal microstructure, and lattice spacing of the samples were examined employing SEM and TEM. According to Fig. S1, the CoFe-LDH precursor showed a layered structure with nano-lamellas stacked with each other. For the CoFeP-m (m = 250, 300, and 350) samples, CoFeP-250 basically maintained the layered structure of CoFe-LDH precursor, and CoFeP-300 showed aggregated nanoparticles that consisted of staggered flakes, while CoFeP-350 exhibited severely agglomerate structure with a rough surface. This phenomenon could be ascribed to the reason that the nanosheet structure of CoFe-LDH collapsed

and aggregated by the influence of PH_3 which was produced by decomposition of NaH_2PO_2 at high temperature in the solid-state reaction process [22]. The microstructures of CoFe-LDH and CoFeP-300 was compared by HRTEM. From the CoFe-LDH TEM picture at 50 nm (Fig. 2a), stacked nanosheets were observed. A high-resolution TEM image at 5nm of this morphology is according to Fig. 2b, and the lattice stripe of 0.25 nm correspond to the (012) crystal plane of CoFe-LDH was detected. Different from the TEM results of CoFe-LDH, CoFeP-300 showed agglomerating structure consisting of small nano-flakes (Fig. 2c). The lattice stripe at 0.20nm was observed at the (110) crystal plane of COP, could be measured by high-resolution image of the CoFeP-300 (Fig. 2d). In addition, the EDS images demonstrated that Co, P, Fe and O, were evenly existence in CoFeP-300 (Fig. 2e).

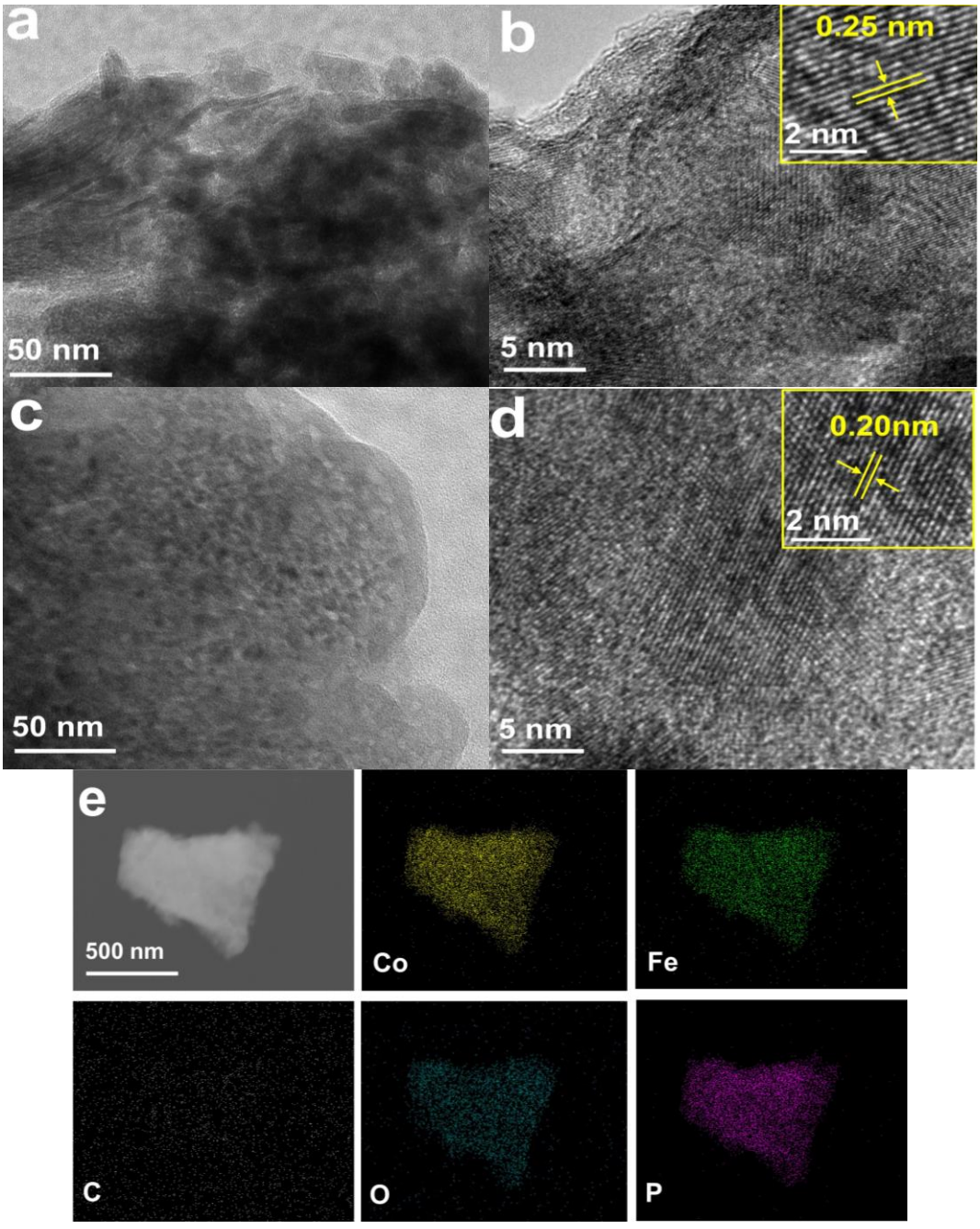

Fig. 2. (HR)TEM images of (a-b) CoFe-LDH, and (c-e) (HR)TEM spectrogram and elemental mappings of CoFeP-300.

To get more insight into the electronic structure and valency chemistry of surface elements of CoFeP-300, a more in-depth study was made on CoFeP-300 by XPS characterization technology. The XPS spectrum (Fig. 3a) showed that Co, O, P and Fe coexist in the composite (O may come from the adsorbed H_2O and CO_2 molecules). The spin-orbit peaks of Co $2p_{3/2}$ and Co $2p_{1/2}$, respectively, may be ascribed to the peaks at 781.4 eV and 797.3 eV in the excellent quality spectrum of Co 2p (Fig. 3b), which are accompanied by two satellite peaks around 786.8 and 803.0 eV. The fitting peaks indicated that Co^{2+} and Co^{3+} coexisted in the sample rate [23]. Fe 2p's spectrum displays two distinct peaks at 712.1 eV and 724.5 eV, which stand for Fe $2p_{3/2}$ and Fe $2p_{1/2}$, respectively, along with a pair of wide satellite peaks at 717.5 eV and 733.1 eV (Fig. 3c). According to the fitting results, the Fe^{2+} and Fe^{3+} coexisted in CoFeP-300 [24]. According to Fig. 3d, the P $2p_{3/2}$ peak at 129.7 eV belongs to the characteristic peak of P-Co/Fe which proves that Co-P and Fe-P coexist in CoFeP-LDH [25], and the wide peak at 133.8 eV is the characteristic peak of P-O, which might be due to the oxidation of the surface of the CoFeP-300 when it was exposed to the air and the surface phosphorus was coordinated with oxygen. According to XPS analysis, there is charge transfer between Co, Fe and P, and the transfer of metal atoms of Co and Fe to P atoms increases the electron transfer rate [25].

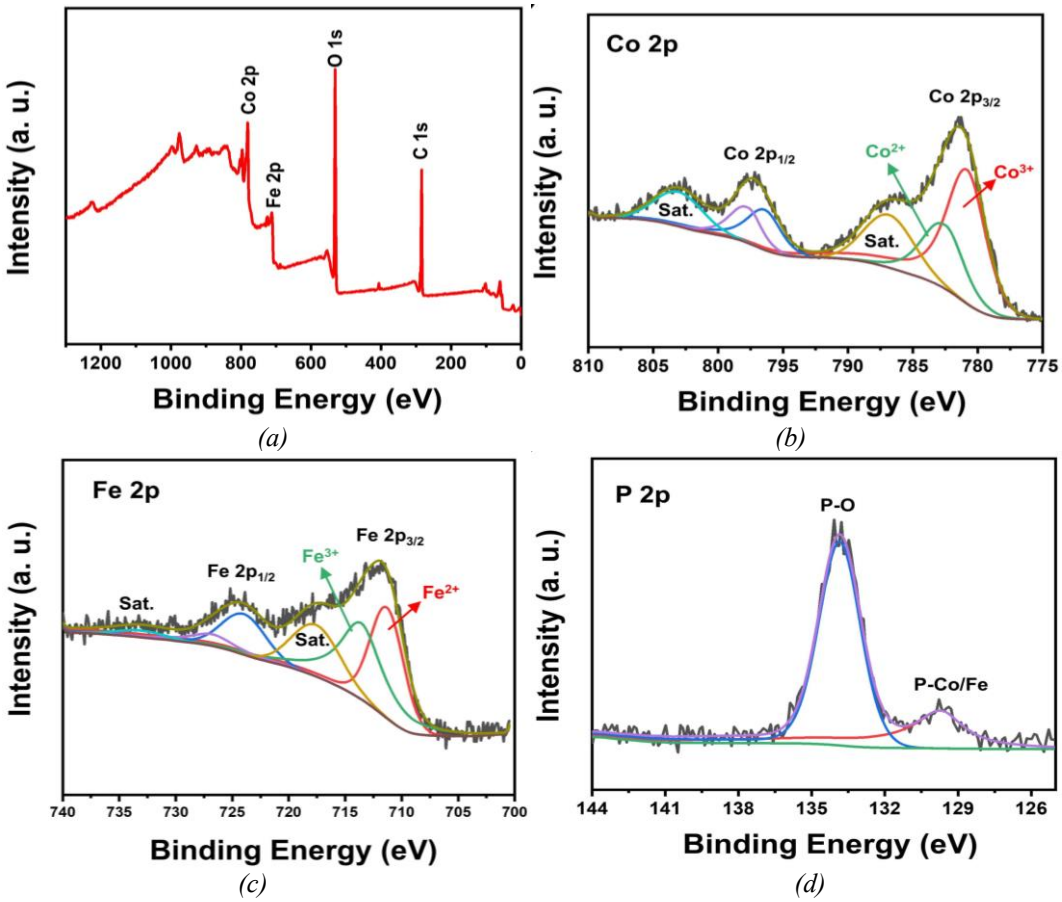

Fig. 3. (a) XPS measurement scanning spectrogram, (b) Co 2p, (c) Fe 2p, and (d) P 2p of CoFeP-300, respectively.

We evaluated the electrochemical properties of CoFe-m materials in a three-electrode standard system (containing 1.0 M KOH+10 mM BA mixed solution). As shown by that cyclic voltammetry (CV) curve of Fig. 4a, all CoFeP-m showed obvious redox peaks of BA, and the peak current density of CoFeP-300 was obviously higher than those of CoFeP-250 and CoFeP-300, which indicated that CoFeP-300 had the strongest electrocatalytic performance for BA oxidation.

The linear sweep voltammetry (LSV) curves in (Fig. 4b) makes this very evident that the current density of CoFeP-300 increased, and at electrical density of 20 mA cm^{-2}, obtained an electromotive force of 1.32 V (V *vs*. RHE), which is much less than that of CoFeP-250 and CoFeP-350, indicating that CoFeP-300 exhibited much higher activity in electrooxidation of BA. The improvement of electrocatalytic performance benefits from lower reaction barrier and Tafel slope. Additionally, Tafel slopes were essential for assessing the kinetics of the electrochemical reaction of the produced CoFeP-m. According to Fig. 4c, the Tafel slope of CoFeP-300 was the smallest, which was 70.02 mV dec^{-1}, fewer than the CoFeP-250 values (181.53 mV dec^{-1}) and CoFeP-350 (139.79 mV dec^{-1}), indicating that CoFeP-300 showed good electrocatalytic oxidation kinetics of BA. The electrode reaction kinetics is generally evaluated by the amount of electric charge transferred, and its value can be conducted by the semicircle in the Nyquist diagram from EIS analyses. The smaller the semicircle is, the faster the reaction speed is. Fig. 4d showed that CoFeP-300 displayed the smallest radius in the above solution, indicating the electron transfer rates was facilitated by CoFeP-300, which promoted the enhancement of catalytic activity for electrooxidation of BA. Additionally, the resistance of the electrolyte (Rs) and the charge transfer resistance (Rct) of the electrochemical procedure (CoFeP-m) were shown in the fitted equivalent circuit diagram (Table S1). Compared to CoFeP-250 (12.52 Ω) and CoFeP-350 (7.77 Ω), CoFeP-300 showed smallest R_{ct} value of 6.39 Ω, suggesting that CoFeP-300 showed faster charge transfer rate and kinetics in the electrooxidation of BA. These unique structures and properties might be ascribed to the appropriate doping of phosphorus, which improves the transfer efficiency of electrons and thus promoting the whole catalytic reaction [26].

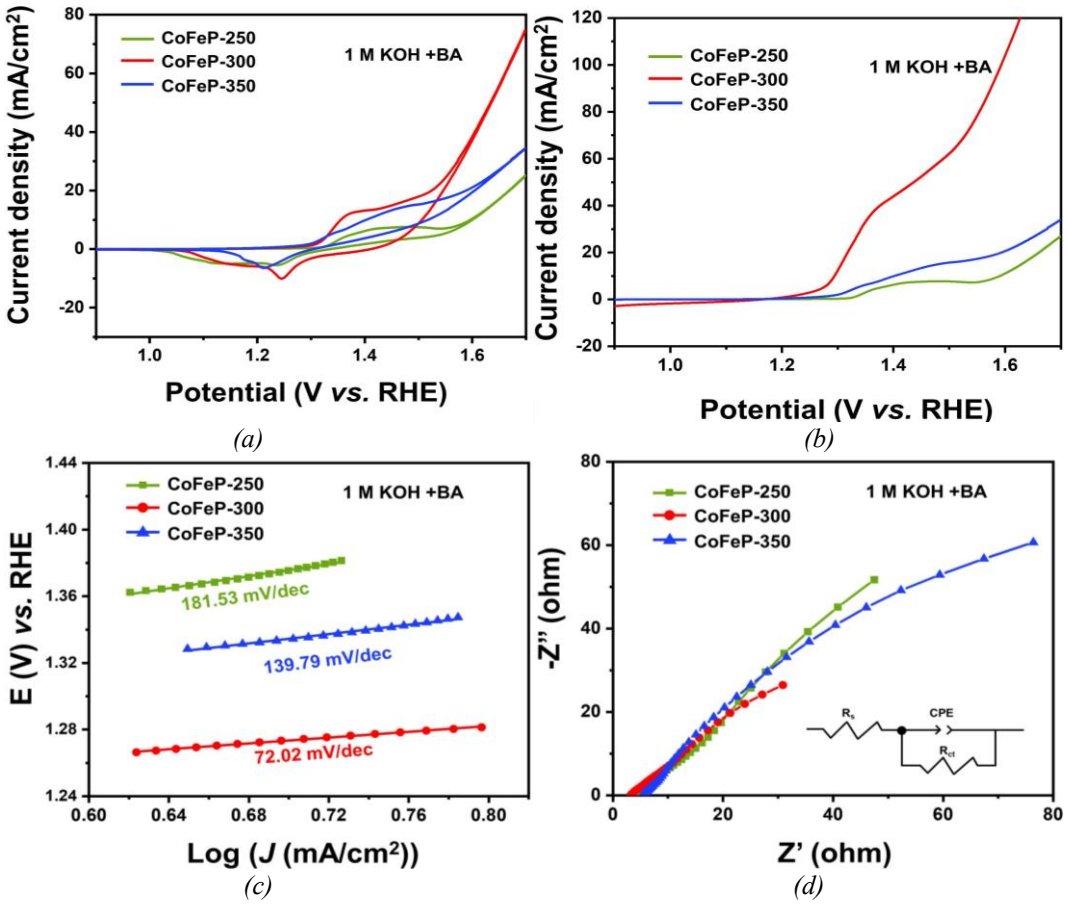

Fig. 4. (a) CV diagram, (b) LSV diagram, and (c) The Tafel slopes at a scanning rate of 5 mV s^{-1} and (d) Nyquist plots of CoFeP-m in 1.0 M KOH with 10 mM BA (the inset was an analogous circuit schematic).

With varying scanning speeds of 2, 4, 6, 8, and 10 mV/s, using the CV of the non-Faraday region in the BA electrolyte, the electrochemical active surface area (ECSA) of CoFeP-m was estimated, more research was done on the impact of the area of surface on electrochemical performance (Fig. S2a-c). The C_{dl} values of CoFeP-250, CoFeP-300 and CoFeP-350 were 128.83 mF/cm^2, 177.08 mF/cm^2 and 163.58 mF/cm^2, respectively. CoFeP-300 possessed the highest C_{dl} value, indicating that CoFeP-300 had higher ECSA and more active centers for BA oxidation, thereby having better electrocatalytic activity. Fast charge transfer resistance, small Tafel slope and high ECSA value of CoFeP-300 make it as a good electrocatalyst for BA oxidation.

Using CoFeP-m as anode to evaluate the electrochemical performance of BA oxidation is mainly due to its unique layered structure. For eight hours, the electrocatalytic experiment was run in the salt solution mentioned above at the ambient temperature, and the concentrations of BA and its oxidation products were quantitatively analyzed by HPLC (Fig. S3). The concentration of BA gradually decreased, and the concentration of benzoic acid, the corresponding main oxidation product, steadily increased as reaction time increased, illustrating that the CoFeP-m material has obvious catalytic activity for BA oxidation. As shown in Fig. 5a, CoFeP-m showed higher activity in electrooxidation of BA than that of CoFe-LDH, suggesting that topological transformation of CoFe-LDH by phosphorylation promoted the electrooxidation of BA [27]. In addition, the selective oxidation of benzyl alcohol to benzoic acid varies with the phosphating temperature in the range of 250 ~ 350 °C: it first increases and then decreases, demonstrating that a proper phosphating temperature could improve the electrooxidation of BA. Specially, CoFeP-300 showed optimal performance of BA electrooxidation (Fig. 5a and 5b, Table S2). Thus, in the subsequent study, CoFeP-300 was employed as an anode to track the electrochemical performance.

The effect of working potentials and recruitment of catalysts on the electrooxidation of BA was further studied. Working potential-wise, 0.40 V–0.80 V *vs*. Ag/AgCl was the range at which the electrooxidation of BA was conducted (Fig. 5c and 5d). It could be seen that increasing working potential was conducive to the progress of the conversion of BA to BAC, and the % transformation of BA and 97.84% BAC's selectivity reached the highest values, which were 97.71% and 97.84% respectively, at the working electromotive force of 0.70 V *vs.* Ag/AgCl. Therefore, the optimized working electromotive force of 0.70 V *vs.* Ag/AgCl was chosen in this research. The influence of the content of catalyst was studied for the electrooxidation of BA by varying the dosage of CoFeP-300 (10, 20, and 30 mg) at voltage of 0.70 V *vs.* Ag/AgCl. As can be seen from Fig. 5e and 5f, the BA (97.71%) and the BAC (97.84%) reached the highest when the dosage of CoFeP-300 was 20 mg. Theoretically speaking, increasing the amount of catalyst could improve the electrocatalytic activity of BA, but when the dosage of CoFeP-300 was increased to 30 mg, the electrocatalytic activity decreases, which might be related to the dosage of Nafion and the NF support with the maximum loading of 1 cm × 1 cm that influenced the catalyst's active sites' interaction with the reactant.

Reusability and stability of the catalysts are of great significance to the environment and economy. The long-term stability and cycle stability of CoFeP-300 were tested. As shown in Fig. 6a and 6b, the BA transform and BAC selectivity of CoFeP-300 maintained 95.89% and 95.37% at the sixth cycles, indicating that the CoFeP-300 showed good cycle stability. The structure of CoFeP-300 after recycled (Re-CoFeP-300) was characterized. As shown in Fig. 6c and 6d, comparing the XRD patterns of CoFeP-300 and Re-CoFeP-300, it is known that their diffraction peaks have not changed significantly, and no new functional groups could be detected in the FTIR spectra of Re-CoFeP-300, demonstrating that following the reaction, the material's crystal structure remained steady. Furthermore, SEM images showed that the morphology of CoFeP-300 remained basically unchanged after the electro oxidation of BA (Fig. S5a-5b). EDX further confirmed that there was no protuberant dissimilarity in the content of element the whole reaction process. The above results show that the layered structure and the addition of phosphorus synergistically promote the electrocatalytic performance of benzyl alcohol oxidation.

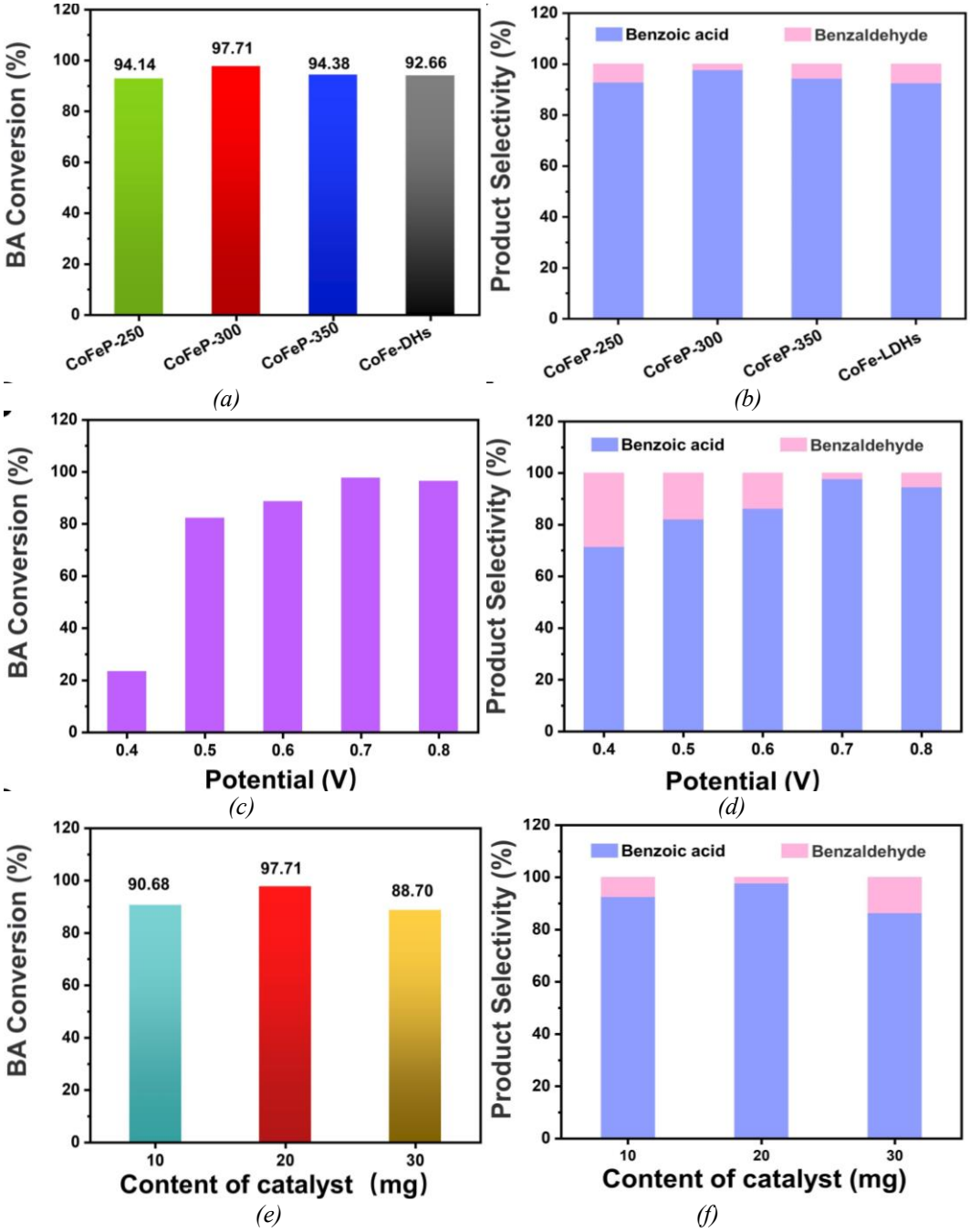

Fig. 5. (a) Selectivity of products and (b) BA conversion across various catalysts. Catalyst 20 mg, 25 °C, 0.70 V vs. Ag/AgCl, and 8 hours are the reaction conditions. (c) BA transform and (d) products selectivity over CoFeP-300 under distinct voltage (0.40 ~ 0.80 V vs. Ag/AgCl). (e) BA conversion and (f) products selectivity with different contents of CoFeP-300.

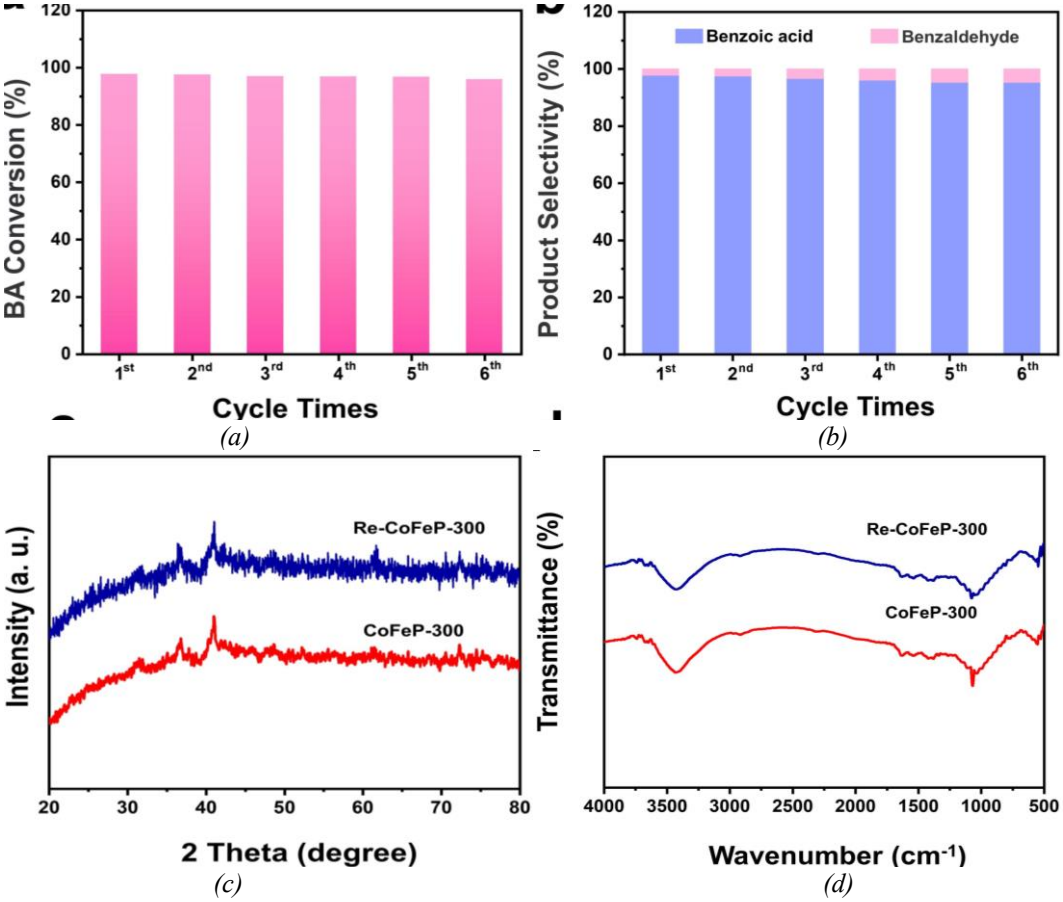

Fig. 6. (a, b) Recycling performance of electrooxidation of BA over CoFeP-300. Reaction conditions: 20 mg CoFeP-300, 25°C, 0.70 V vs. Ag/AgCl, 8 h. (c) XRD spectrogram and (d) FTIR spectrum of Re-CoFeP-300.

The electrooxidation of BA was carried out in aqueous solution system, and the oxidation of water might hinder the catalytic oxidation. According to Fig. 7a, the CV curve of CoFeP-300 measured in the containing benzyl alcohol showed an obvious oxidation peak at 1.37 V *vs.* RHE, and the peak current intensity increased obviously with the increasing of potential, indicating that CoFeP-300 had strong electrocatalytic performance for BA oxidation. The LSV curve shows that CoFeP-300 achieved the voltage of 1.62 V *vs.* RHE at the present density of 50 mA/cm^2 in 1.0 M KOH solution. In the electrolyte containing 10 mM BA, the potential decreased to 1.43 V *vs.* RHE at the same current density, suggesting that CoFeP-300 had certain electrocatalytic oxidation ability for benzyl alcohol. The Tafel slopes of CoFeP-300 for electrooxidation of BA is 70.02 mV dec^{-1}, which was below the level of OER (80.08 mV dec^{-1}) (Fig. 7c), indicating that CoFeP-300 showed superior electrooxidation kinetics of BA. The C_{dl} of CoFeP-300 for electrooxidation of BA (177.08 mF/cm^2) was larger than that for OER (119.6 mF/cm^2) (Fig. 7d and S5), which further proved that electro oxidation of BA was easier in this system.

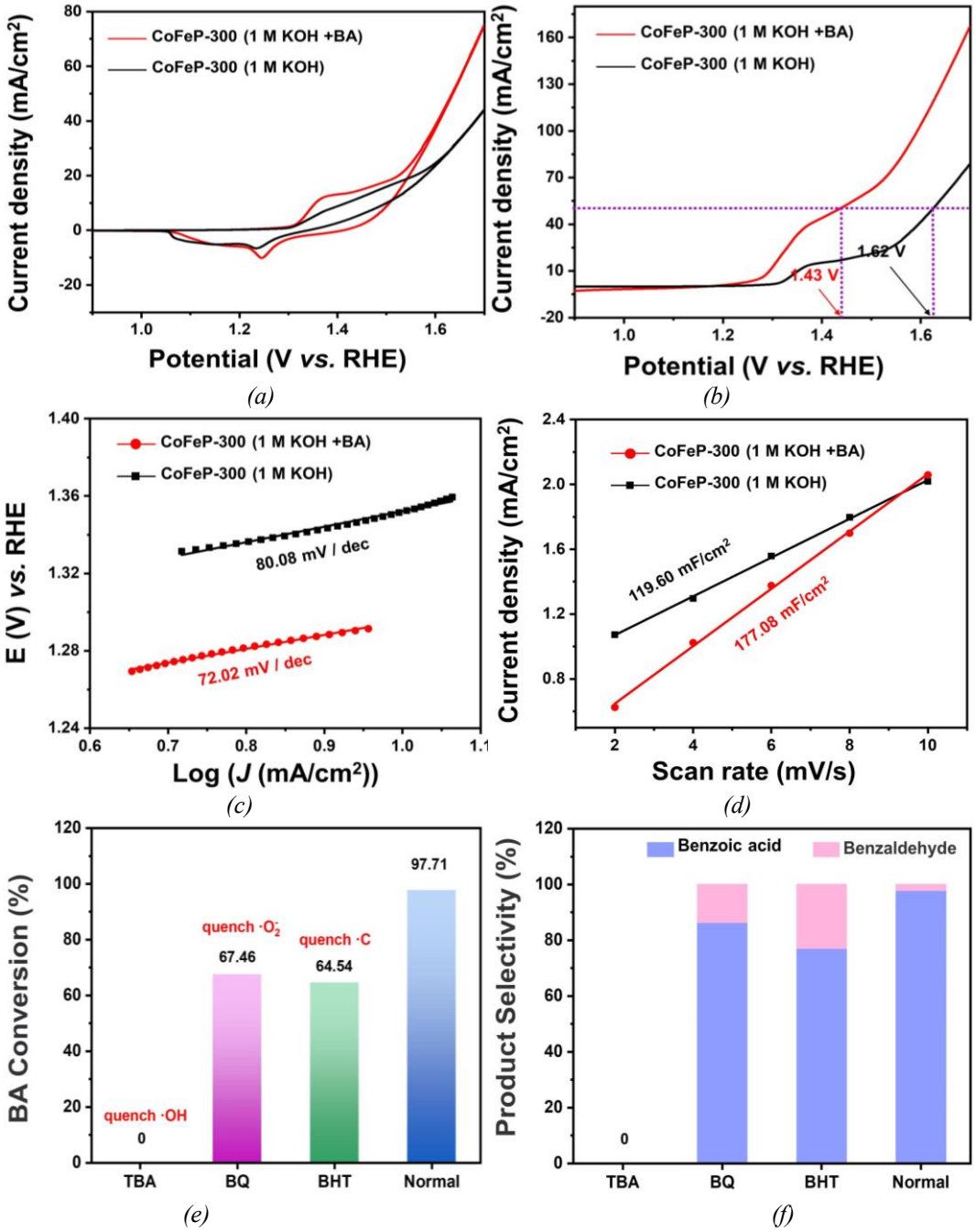

Fig. 7. (a) CV curves, (b) LSV curves, and (c) Tafel slopes of CoFeP-300 reaction conditions: scanning rate of 5 mV s-1, presence and absence of BA solution. (d) double-layer capacitor (C_{dl}). (e-f) The effect of different free radical trapping agents on electrocatalytic oxidation of benzyl alcohol.

In the previous experiments [20], it had been proved that the active free radicals involved in the reaction in the catalytic oxidation system of BA were carbon center free radicals (R·), to ascertain the respective contributions of hydroxyl (·OH) and superoxide ($\cdot O_2^-$) free radicals, a quenching experiment was carried out [28]. Fig.7e-f revealed how various scavengers affected the pace at which BA was catalyzed to oxidize in less than eight hours, and it could be seen that adding catalysts could obviously inhibit the electrooxidation rate of BA. After adding tert-butyl alcohol (TBA), the transform of benzyl alcohol was obviously restrained, which indicated that hydroxyl radical (·OH) is an indispensable substance in the electrooxidation process of BA. After adding p-benzoquinone (BQ) and butyl hydroxytoluene (BHT), the electrooxidation of BA was

partially inhibited, and the transform of BA diminished to 67.46% and 64.54%, respectively, while the selectivity of BAC diminished to 86.33% and 77.1%, respectively. The results showed that there were both $\cdot O_2^-$ and R· involved in the reaction system. These showed that the exceptional electrochemical performance of CoFeP-300 was derived from the joint action of various free radicals.

4. Conclusion

To sum up, CoFe bimetallic phosphide (CoFeP-m) electrocatalysts was obtained through topological transformation of CoFe-LDH precursor by phosphating NaH_2PO_2 at different temperatures. Benefiting from the bimetallic synergy, fully exposed active sites, increased conductivity, and fast charge transfer, the CoFeP-m realized efficient BA conversion with high BAC selectivity. Specially, CoFeP-300 showed best electrocatalytic performance of BA oxidation among the CoFeP-m catalysts, where the transform of BA and BAC selectivity achieved 97.71% and 97.84% at the operational voltage of 0.7 V *vs*. Ag/AgCl for 8 h under room temperature. Furthermore, CoFeP-300 exhibited good stability, maintaining 95.89% transform of BA and 95.37% BAC's selectivity at the sixth cycle. A novel method for electrotonizing BA employing transition metal phosphide electrode materials is presented in this work.

Acknowledgements

The National Natural Science Foundation of China (No.: 42062003) is funding this research, the Guangxi Natural Science Foundation (No. 2023GXNSFBA026183), the Research Foundation of Key Laboratory of New Processing Technology for Nonferrous Metal & Materials, Ministry of Education/Guangxi Key Laboratory of Optical and Electronic Materials and Devices (No. 23AA-6), the Open Project of Guangxi Key Laboratory of Nuclear Physics and Nuclear Technology (No. NLK2022-08).

References

[1] J. Zhong, Y. L. Shen, P. Zhu, S. Yao, Nano Research **16**(1), 202 (2022); http://doi.org/ 10.1007/s12274-022-4679-6
[2] M. Xu, J. Geng, H. Xu, S. B. Zhang H. M. Zhang, Inorganic Chemistry Frontiers **10**, 2053 (2023); http://doi.org/ 10.1039/d2qi02526d
[3] L. H. Liu, N. Li, J. R. Han, K. L. Yao, H.Y. Liang, International Journal of Minerals, Metallurgy and Materials **29**(3), 503 (2022); http://doi.org/10.1007/s12613-021-2352-9
[4] J. H. Shi , P. Wei, Y. F. Yang, B. Li, J. H. Nie, H. Wan, Y. Li, G. F. Huang, W. Y. Hu, W. Q. Huang, Small **19**(30), 2302906 (2023); http://doi.org/10.1002/smll.202302906
[5] S. H. Bae, J. E. Kim, H. Randriamahazaka, S. Y. Moon, J. Y. Park, I. K. Oh, Advanced Energy Materials **7**(1), 1601492 (2016); http://doi.org/10.1002/aenm.201601492
[6] X. Xiao, L. M. Tiao, M. Li, X. W. Lv, D. K. Huang, X. X. Jiang, H. P. Pan, M. K. Wang, Y. Shen, Chemical Science, **9**, 1970 (2018); https://doi.org/10.1039/C7SC04849A
[7] D. Y. Chung, S. W. Jun, G.Yoon, H. Kim,J. M. Yoo, K. S. Lee, T. Kim, H. Shin, A. K. Sinha, S. G. Kwon, K. Kang, T. Hyeon, Y. E. Sung, Journal of the American Chemical Society **139**(19), 6669 (2017); https://doi.org/10.1021/jacs.7b01530
[8] Y. B. Lian, H. Sun, X. B. Wang, P. W. Qi, Q. Q. Mu, Y. J. Chen, J. Ye, X. H. Zhao, Z. Deng, Y. Peng, Chemical Science **10**, 464 (2018); https://doi.org/10.1039/C8SC03877E
[9] C. C. Du, M. X. Shang, J. X. Mao, W. B. Song, Journal of Materials Chemistry A **5**, 15940 (2017); https://doi.org/10.1039/C7TA03669H
[10] J. Y. Li, M. Yan, X. M. Zhou, Z. Q. Huang, Z. M. Xia, C. R. Chang, Y. Y. Ma, Y. Q. Qu, Advanced Functional Materials **26**(37), 6673 (2016); https://doi.org/10.1002/adfm.201601420

[11] X. Zhang, J. W. Li, Y. F. Sun, Z. J. Li, P. Liu, Q. Y. Liu, L. Tang, J. X. Guo, Electrochimica Acta **282,** 626 (2018); https://doi.org/10.1016/j.electacta.2018.06.099
[12] S. K. T. Aziz, S. Sultana, A. Kumar, S. Riyajuddin, M. Pal, A. Dutta, Cell Reports Physical Science **4**(12), 101747 (2023); https://doi.org/10.1016/j.xcrp.2023.101747
[13] V. Jain, Y. Bonita, A. Brown, A. Taconi, J. C. Hicks, N. Rai, Catalysis Science and Technology **8**, 4083 (2018); https://doi.org/10.1039/C8CY00977E
[14] D. P. Sahoo, K. K. Das, S. Mansingh, S. Sultana, K. Parida, Coordination Chemistry Reviews **469**, 214666 (2022); https://doi.org/10.1016/j.ccr.2022.214666
[15] M. M. Rajpure, H. S. Jadhav, H. Kim, Colloids and Surfaces A: Physicochemical and Engineering Aspects **654**, 130062 (2022); https://doi.org/10.1016/j.colsurfa.2022.130062
[16] U. A. Mohanty, D. P. Sahoo, L. Paramanik, K. Parida, Sustainable Energy and Fuels **7**, 1145 (2023); https://doi.org/10.1039/D2SE01510B
[17] M. Rinawati, Y. X. Wang, K. Y. Chen, Chemical Engineering Journal **423**, 130204 (2021); https://doi.org/10.1016/j.cej.2021.130204
[18] H. L. Liu, T. T. Yu, D. Q. Su, Z. H. Tang, J. H. Zhang, Y. J. Liu, A. H. Yuan, Q. H. Kong, Ceramics International **43**(16), 13031 (2017); https://doi.org/10.1016/j.ceramint.2017.07.207
[19] J. Xie, Z. Khalid, J. M. Oh, Bulletin of the Korean Chemical Society **44**(2), 100 (2022); https://doi.org/10.1002/bkcs.12649
[20] Y. Q. Xu, H. J. Liu, Y. X. Wu, Q. Wu, C. J Li, X. Y. Wang, H. Q. Qin, A. M. Qin, L. J. Wang, ChemNanoMat **9**(12), 0414 (2023)
[21] A. Hameed, M. Batool, Z. Y. Liu, M. A. Nadeem, and R. C. Jin, ACS Energy Letters **7**(10) 3311 (2022); https://doi.org/10.1021/acsenergylett.2c01362
[22] R. Yang, Y. M. Zhou, Y. Y. Xing, D. Li, D. L. Jiang, M. Chen, W. D. Shi, S. Q. Yuan, Applied Catalysis B: Environmental **253**(15), 131 (2019); https://doi.org/10.1016/j.apcatb.2019.04.054
[23] Y. Y. Xie, H. F. Huang, Z. D. Chen, Z. J. He, Z. X. Huang, S. L. Ning, Y. N. Fan, M. Barboiu, J. Y. Shi, D. W. Wang, C. Y. Su, Inorganic Chemistry **61**(21), 828, (2022); https://doi.org/10.1021/acs.inorgchem.2c00727
[24] X. T. Yu, M. Y. Wang, X. Z. Gong, Z. C. Guo, Z. Wang, S. Q. Jiao, Advanced Energy Materials **8**(34), 1802445 (2018); https://doi.org/10.1002/aenm.201802445
[25] S. H. Wang, P. Yang, X. F. Sun, H. L. Xing, J. Hu, P. Chen, Z. T. Cui, W.K. Zhu, Z.J. Ma, Applied Catalysis B: Environmental **297**(15), 120386 (2021); https://doi.org/10.1016/j.apcatb.2021.120386
[26] W. Zhan, L. Ma, M. Y. Gan, F. Xie, Applied Surface Science **585**, 152621(2022); https://doi.org/10.1016/j.apsusc.2022.152621
[27] S. F. Sun, M. Zheng, P. F. Cheng, F. G. Wu, L. P. Xu, Journal of Colloid and Interface Science **626**, 515 (2022); https://doi.org/10.1016/j.jcis.2022.06.053
[28] R. Gao, D. P. Yan, Nano Research **11**(4), 1883 (2018); https://doi.org/10.1007/s12274-017-1806-x